Percolation based architecture for cluster state quantum computation using photon-mediated entanglement between atomic memories

Mihir Pant,[1,2,*] Hyeongrak Choi,[1,*] Saikat Guha,[2] and Dirk Englund[1]

[1] *Research Laboratory of Electronics, Massachusetts Institute of Technology, Cambridge, Massachusetts, 02139, United States*
[2] *Quantum Information Processing Group, Raytheon BBN Technologies, 10 Moulton Street, Cambridge, Massachusetts 02138, USA*

arXiv:1704.07292v1 [quant-ph] 24 Apr 2017

We propose an on-chip scalable cluster-state quantum computing (QC) architecture comprising a two-dimensional array of atomic qubits and detectors, networked by photonic switches and waveguides. A major barrier to scaling up such systems lies in efficiently entangling neighboring atomic memories by conversion of the qubits to photons and establishing entanglement via Bell measurements in the optical domain, all within the coherence time. Our architecture leverages percolation theory to significantly reduce the time required to create a universal-QC-capable cluster of atomic memories, compared with recently-studied architectures that rely on repeat-until-success entanglement connections. This reduction puts our architecture in an operational regime where demonstrated collection, coupling and detection efficiencies would be sufficient for scalable QC with experimentally demonstrated coherence times. Furthermore, our approach dispenses the need for time consuming feed-forward, high-cooperativity interfaces and ancilla single photons, and can also tolerate a high rate of site imperfections. We also propose a variant of the architecture which allows for long-range connections and makes our architecture even more resilient to low site yields. We analyze our architecture for nitrogen-vacancy (NV) centers in diamond, but emphasize that the approach applies to any atomic or atom-like system.

The past years have seen rapid advances in controlling small groups of qubits encoded in atomic or atom-like quantum memories. An important question now concerns the development of architectures to efficiently combine these memories into large-scale systems capable of general-purpose quantum computing [1–4]. A promising approach is entangling the atomic qubits with optical links to generate so-called cluster states, and then computing with adaptive measurements (one-way quantum computing) [5]. A key challenge is to produce this cluster state fast enough to allow the one-way quantum computing and error correction within the finite coherence time of the memory.

Here, we show that percolation of heralded entanglement allows us to create arbitrarily large cluster states, which are a resource for universal quantum computation. This process is fast enough for implementation with device parameters that have been demonstrated; one does not need high cooperativity cavities, ancilla single photons, or time-consuming feed-forward operations. Furthermore, as opposed to previous schemes, we do not require error correction to account for missing bonds, and instead use renormalization [6–8] which can be done with constant overhead [9] if the bond probability exceeds the percolation threshold. The percolation approach also provides tolerance for site imperfections in several different lattice architectures. When combined with our novel transparent node architecture which allows long range connections, a further reduction in the percolation threshold can be achieved. We also found a theoretical limit of the percolation threshold across different geometries, and found that our proposed geometries are within a factor 1.6 of the limit. Our approach applies to a number of leading physical qubit systems, including atomic gases [10], ion traps [11] or rare earth ions [12], though for clarity, we focus here on nitrogen vacancy (NV) centers in diamond.

NV centers in diamond have many properties that make them favorable as a quantum memories. The NV^- charge state has a robust optical transition for heralded entanglement between distant NV centers [13, 14] and a long electronic spin (S=1) coherence time [15] for high-fidelity qubit operations. Recently, single qubit gates with fidelities up to 99% have been achieved with optimal control techniques [16]. They can be coupled with surrounding nuclear spins [17], which have coherence times exceeding one second even at room temperature [18]. The electronic spin state can be transferred to the nuclear spin, and single shot measurement of nuclear spin is possible by repetitive measurement of the electron spin [19]. In addition, the fact that the memories are solid state and can be coupled with integrated photonic devices [20] makes it a promising platform for large scale quantum computation.

Fig. 1 illustrates the percolation approach to cluster state generation with quantum memories. We work in the framework of cluster states where nodes represent qubits in the state $(|0\rangle + |1\rangle)/\sqrt{2}$ and edges/bonds represent controlled-Z (CZ) gates between neighboring nodes. Consider a square lattice where every edge exists with probability p as shown in Fig. 1(a)-(c). The computational power of such a system is related to the size of the largest connected component (LCC) in the cluster (shown in red). When $p < 0.5$, the clusters form small disconnected islands. In this regime, for a lattice with N nodes, the size of the LCC is $O(\log(N))$ [21]. Local measurements on such a lattice can be efficiently simulated

* These authors contributed equally to this work

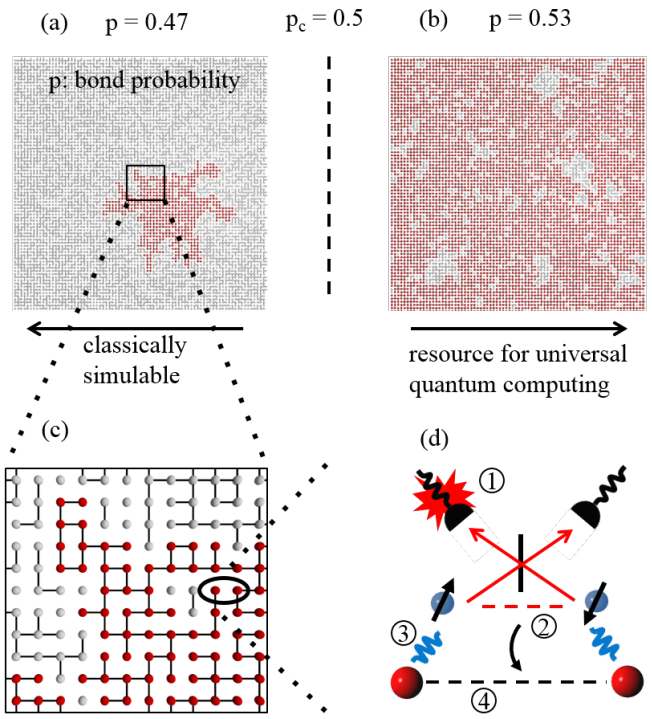

FIG. 1. Cluster state generation by percolation. (a),(b) Transition in the size of the largest connected component (LCC) with increasing bond probability. Spheres and lines represent nodes and bonds respectively, and the red spheres represent the LCC. When the bond probability (p) goes above the percolation threshold (p_c), the size of the LCC suddenly increases and the cluster changes from being classically simulable to a resource for universal quantum computation. (c) Expanded view of (a). (d) Physical implementation of nodes and bonds with NV centers in diamond. ① Probabilistic Bell measurement (Barret-Kok protocol) is attempted on two nearest-neighbor broker qubits (electronic spins, blue spheres). ② Conditioned on one photon detection events, the two broker qubits are entangled onto a Bell state. ③ Hyperfine interaction between electronic spins and nuclear spins (client qubits, ^{15}N) mediates controlled-Z gates. ④ X-basis measurement of electronic spins projects nuclear spins into an entangled state heralded by the measurement results (entanglement swapping)

classically and hence, the resource is not good enough for quantum computing [22]. When the bond probability exceeds 0.5 there is a sudden transition in the size of the LCC: the number of nodes in the LCC is now $\Theta(N)$. This is accompanied by a sudden transition in computational power; single qubit adaptive measurements on this cluster have the power of universal quantum computing [9]. The bond probability p_c at which the transition takes place is called the percolation threshold. Square, triangular and hexagonal lattice clusters above the percolation threshold are resources for universal quantum computation [6, 9], although there are examples of other lattices for which this is not true e.g. Bethe lattice clusters are not resources for universal quantum computation [23].

Figure 1(d) shows the physical implementation of the link creation with NVs. The nuclear spins (red spheres) function as "client qubits" that store entanglement. They are coupled to the NV electronic spins - "broker qubits" - that are entangled remotely by Bell measurements mediated by photons. In each time step, we attempt to create one edge (entanglement) at each node by heralded entanglement mediated by photons. To be specific, we consider the Barret-Kok entanglement protocol [24] on the broker qubits of neighboring nodes/sites. If the probabilistic Bell measurement succeeds, the electron spins of the corresponding NVs are entangled. This entanglement is then transferred to the nuclear spin with an entanglement swapping procedure, as illustrated in Fig. 1(f) and described in detail in the supplementary material [25] and Ref. [1]. The whole cycle from initialization to entanglement swapping takes approximately $t_0 = 5$ μs based on recent experimental demonstrations [14] [25].

The Barret-Kok protocol to generate entanglement is advantageous because it does not require ancilla single-photons or high cooperativity cavities [1]. Furthermore, photon loss in this scheme does not degrade fidelity, which is critical to the error correction overhead. This increased fidelity comes at the price of low bond success probability (detailed in Table I) which is a problem for conventional architectures. This can be overcome in our percolation based architecture.

The bond lengths could practically be very short, on the order of tens of microns, and the entire cluster may be integrated on a chip, as illustrated in Fig. 2. Each node in the architecture requires atomic memory and a $1 \times d$ switch, where d is the degree of the lattice being attempted (4 for the square lattice). Each edge in the lattice requires waveguides between the nodes, a beam-splitter and two detectors to implement the Bell measurement.

At each time step in the operation of the system, each atomic memory generates a photon entangled with the electron spin which is routed towards one of the d neighbors for the Bell measurement, so that for n_{att} time steps for entanglement generation, entanglement with each of the d neighbors of a node is attempted n_{att}/d times. It is important to synchronize neighboring switches such that both photons required to attempt an edge arrive at the same time. For the hexagonal ($d = 3$), square ($d = 4$) and triangular ($d = 6$) lattices, synchronization is straight-forward. Each switch only needs to be flipped $d-1$ times during entanglement creation, and hence the switching time is negligible.

The probability of successfully heralding the entanglement of two NV centers is $p_0 = \eta^2/2$ [24], where η is the efficiency of emitting, transmitting, and detecting the photon entangled with the electronic spin (zero phonon line, ZPL) from the NV excited state. Table I summarizes p_0 for three representative types of NV-photon interfaces: low-efficiency interfaces with $p_0 = 5\times10^{-5}$ representative of today's state of the art Bullseye grating or solid immersion lenses (SILs) [14, 26, 27]), medium $p_0 = 2\times10^{-4}$

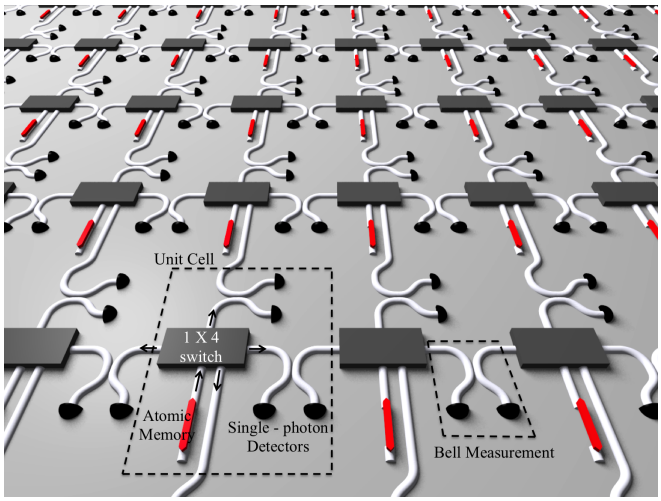

FIG. 2. Physical implementation of the proposed architecture. A unit cell consists of an atomic memory, a 1×4 switch, waveguides and 4 single-photon detectors. Single-photons emitted from the atomic memory are coupled to the waveguide and directed to the switch. The switch chooses one of the nearest-neighbor nodes to be entangled with, and single-photons are interfered using a 50/50 beam-splitter. Single-photon detectors detect interfered photon projecting electronic spins onto an entangled state.

for NV centers coupled to diamond waveguides [20], and high efficiency $p_0 = 5 \times 10^{-2}$ for nanocavity-coupled NV centers coherently interacting with each other [28]. For all three coupling mechanisms, we have assumed coupling efficiencies that have already been demonstrated experimentally (see supplementary information for more details [25]). After n_{att}/d entanglement attempts with a nearest neighbor, the probability of having generated a bond is $p = 1 - (1 - p_0)^{n_{\text{att}}/d}$.

Based on the entanglement success probability per attempt, we performed simulations using the Newman-Ziff algorithm [29] with 9 million nodes to evaluate the growth of the clusters. Fig. 3(a) plots the fraction of nodes that are within the largest cluster component (f_{LCC}), as a function of time, assuming $t_0 = 5$ μs. In Fig. 3(a), the underlying geometry is a square lattice. The lines represent different Bell measurement success probabilities corresponding to the coupling mechanisms in table I. Initially, f_{LCC} is $\text{O}(\log(N)/N)$ [21] where N is the total number of nodes in the lattice. As the bond success probability passes the bond percolation threshold (p_c), f_{LCC} rapidly rises and becomes $\Theta(1)$. For a degree d lattice, the bond probability after time t is $p = 1 - (1 - p_0)^{t/t_0 d}$. From this, we can calculate that the time required to obtain a resource for universal quantum computation is $t_c = t_0 d \ln(1 - p_c)/\ln(1 - p_0)$, which is depicted with the vertical dashed lines in the figure. The transition becomes sharper as the number of nodes in the lattice (N) increases.

TABLE I. Bell measurement success probability (p_0), Bond trial time (t_0) and readout time for three different coupling schemes

Collection	Bullseye or SIL	Waveguide	Cavity
Bond success prob. p_0	5×10^{-5}	2×10^{-4}	5×10^{-2}
Bond trial time t_0[a]	5 us	5 us	5 us
Readout time	4 us	800 ns	400 ns

[a] including state initialization

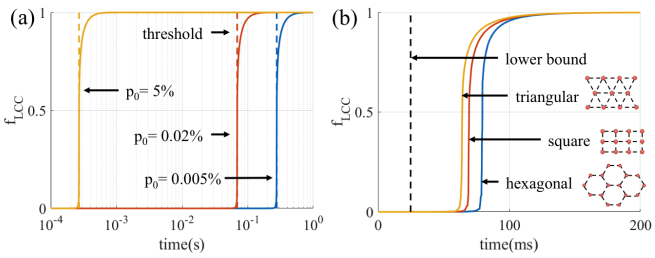

FIG. 3. Size of the largest connected component vs time for (a) different values of p_0, the probability of successful Bell measurement in one attempt and (b) different underlying lattice geometries. A square lattice is used in (a) and $p_0 = 0.02$ % is used for (b).

In all three collection schemes, the bond success probability exceeds the percolation threshold within the experimentally demonstrated coherence time of the nuclear spins of the NV: 1 second. We find a surprising result; even with free space coupling without any ZPL enhancement, an arbitrarily large cluster can be generated.

It is well known from percolation theory that higher connectivity between nodes can reduce the percolation threshold. Does the time to exceed threshold (t_c) change significantly with the lattice degree d? As shown in Figure 3(b), which plots f_{LCC} for two additional lattice types, triangular ($d = 6$) and hexagonal ($d = 3$), t_c is nearly the same for the three lattice types. Although increasing d does lower the bond percolation threshold, it also decreases the number of entanglement attempts between NVs, which is n_{att}/d. This is because a single broker qubit per NV requires entanglement attempts to proceed serially. Increasing d would in fact substantially lower t_c if each site contained d broker qubits that could be entangled simultaneously.

Let us consider the most general scenario where there is full controllable connectivity in the graph, i.e., we can attempt Bell measurements on any pair of NVs in a time step. What is the minimum time, $t_c^{(LB)}$ ($\min(t_c)$), required to obtain a resource for universal quantum computation, optimizing over all lattice geometries, if the bonds are attempted without feed-forward? The bond probability after time t is $p = 1 - (1 - p_0)^{t/t_0 d}$. For percolation, $p \geq p_c$ i.e. $t_c \geq dt_0 \ln(1 - p_c)/\ln(1 - p_0)$. For a degree d lattice, $p_c \geq 1/(d - 1)$ [30, 31], with equality for a degree d Bethe lattice. This leads to $t_c \geq dt_0 \ln(1 - 1/(d - 1))/\ln(1 - p_0)$. t_c is minimized as $d \to \infty$ in which case we obtain $t_c^{(LB)} = -t_0/\ln(1 - p_0)$

which is the minimum possible time required to generate a resource for universal quantum computing without feed-forward. $t_c^{(LB)}$ is plotted as a black dashed line in Fig. 3(b). The lattice corresponding to this threshold is the infinite-dimensional, infinite degree Bethe lattice which is clearly impractical and also not a resource for universal quantum computing [23]. Yet, we find that the simple 2D lattices with nearest neighbor connectivity we chose in Fig. 3 are only a factor 3 above this limit and are resources for universal quantum computing.

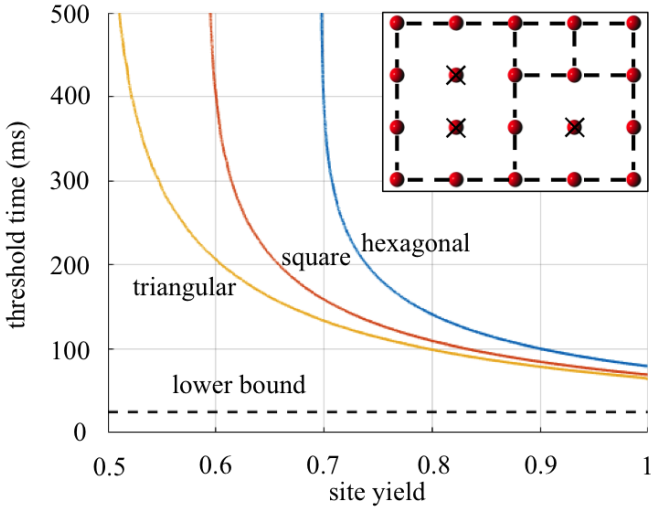

FIG. 4. The minimum time required to obtain a percolated lattice with sub-unity site-yield. $p_0 = 0.02\%$. The inset shows the bonds that can be attempted in a square lattice if the sites marked with crosses are inactive

Experimentally, it is important to consider the effect of non-functional sites (e.g. a far-detuned NV center or a missing trapped ion). Even if all faulty nodes and their edges are removed, as illustrated in Fig. 4(a), the lattice can retain enough bonds to give a percolated cluster. In this case, the problem maps to site-bond percolation. This is quantified in Fig. 4 where we plot the minimum time required to obtain a percolated cluster as a function of the site-yield (q), assuming NVs coupled to diamond waveguides without a cavity (medium $p_0 = 0.02\%$). In general, a reduced site-yield can be compensated with a larger bond probability which corresponds to more time. While the hexagonal, square and triangular lattices have a similar threshold time t_c when the site-yield is perfect, the tolerance to imperfect site-yield is different. Following the trend of the site percolation threshold (q_c), the triangular ($q_c = 0.5$) performs better than square ($q_c \approx 0.593$), which performs better than the hexagonal lattice ($q_c \approx 0.697$). The site percolation threshold corresponds to the minimum possible site-yield for percolation with all bonds having succeeded ($p = 1$).

The architecture that we have discussed thus far allows for only nearest neighbor connections between atomic memories. In Fig. 5, we present a modified architecture that can be used to make long range connections which can in turn decrease the threshold time and increase tolerance to imperfect site yield. Furthermore the architecture reduces the required number of detectors by a factor of 4. In this architecture (Fig. 5(a)), the 1×4 switch from Fig. 2 is replaced by a 5×5 Mach-Zehnder interferometer (MZI) array with the input and output ports depicted with arrows in the unit cell. The 5×5 MZI array can be used to implement any linear optic unitary between the set of input and output modes [32]. On-chip fully-programmable MZI arrays of 22 input and output modes [33] have been demonstrated. The MZI arrays allow us to make long range connections by turning nodes "transparent" and entangle distant nodes while maintaining a planar physical architecture.

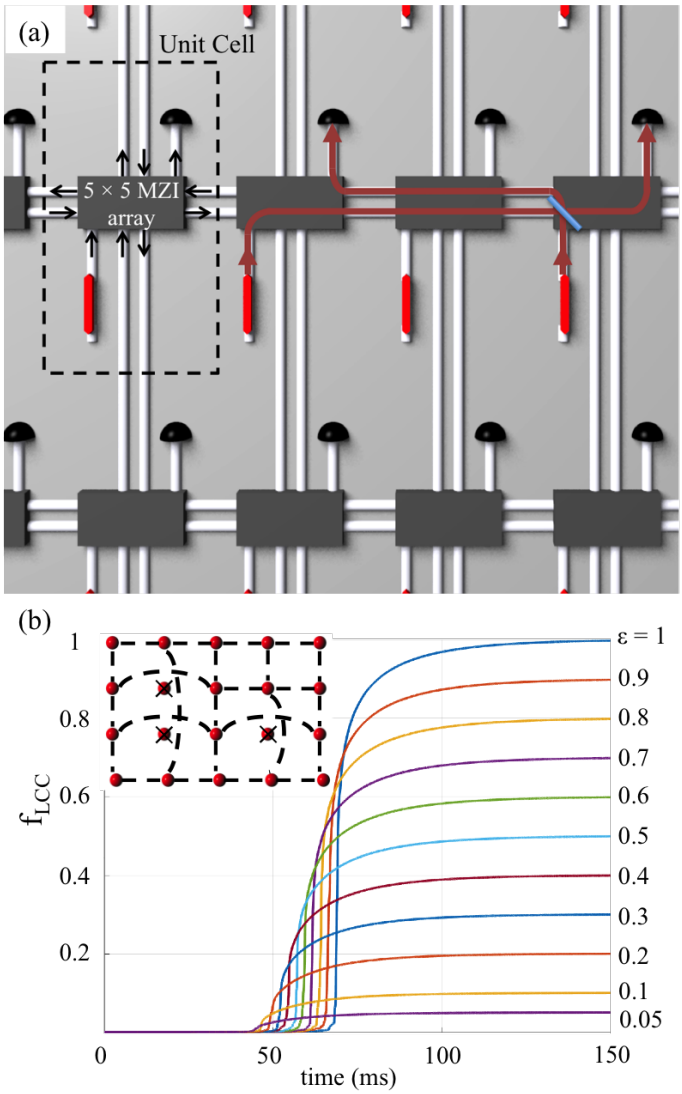

FIG. 5. (a) A more general architecture with switches replaced by MZI arrays can allow for long-range entanglement as shown here (b) f_{LCC} as a function of time for different values of ϵ. $p_0 = 0.02\%$ is used here.

One way to use this more general architecture is to

randomly turn a fraction $1-\epsilon$ of the nodes transparent as shown in the inset of Fig. 5(b). The resulting plot of f_{LCC} vs time with $N = 9$ million nodes is shown in Fig. 5(b). As ϵ decreases starting from one, the maximum possible value of f_{LCC} is also reduced from one to ϵ because only a fraction ϵ nodes have active qubits. However, because the transparent nodes increase dimensionality while maintaining connectivity, reducing ϵ actually reduces the t_c at which we obtain a $\Theta(N)$ connected cluster for universal quantum computation. Therefore, for a given entanglement generation time, there is an optimum value of ϵ which gives us the largest LCC. We numerically found that the minimum possible bond percolation threshold in the transparent architecture is ≈ 0.33 which is achieved when $1/N \ll \epsilon \ll 1$ i.e. when $\epsilon \to 0$ but the number of non-transparent nodes in the lattice is still $\Theta(N)$. Faulty sites can be incorporated into the fraction of transparent nodes as long as the yield $\gg 1/N$ without affecting the minimum entanglement time t_c.

In conclusion, we proposed an architecture for quantum computing with atomic memories that uses the concept of percolation to produce a resource for universal quantum computing within the coherence time of the NV nuclear spins, even with imperfect site-yield. Compared to previous scheme which require repeating each bond a large number of times to obtain a bond probability of $p > 0.999$, we find that the required number of attempts is reduced by an order of magnitude, which lowers the requirement on memory coherence time by the same factor. Furthermore, the missing bonds are resolved using renormalization rather than error correction, which can be done with constant overhead. Our scheme does not need high cooperativity cavities or ancilla single photons, and minimizes the amount of feed-forward. The proposed blueprint is applicable to arbitrarily large numbers of qubits. For example, in the planar platform outlined in Fig. 5(a), with a realistic lattice spacing of 10-20 m, a centimeter-scale chip could accommodate on the order of a million qubits. Future work should focus on determining the most efficient algorithm and calculating the constant resource overhead required to renormalize a percolated lattice in the form of a quantum error correction code. Because of our architecture's natural tolerance to faulty sites and missing bonds, the size of the required error correction code can be expected to be smaller than conventional architectures.

ACKNOWLEDGMENTS

M.P., H.C. and D.E. acknowledge support from the Air Force Office of Scientific Research MURI (FA9550-14-1-0052). H.C. was also supported in part by a Samsung Scholarship. S. G. acknowledges support from the Office of Naval Research MURI (N00014-16-C-2069).

M.P. and H.C. have contributed equally to this work.

[1] K. Nemoto, M. Trupke, S. J. Devitt, A. M. Stephens, B. Scharfenberger, K. Buczak, T. Nöbauer, M. S. Everitt, J. Schmiedmayer, and W. J. Munro, Physical Review X **4**, 031022 (2014), arXiv:1309.4277.

[2] C. Monroe, R. Raussendorf, A. Ruthven, K. R. Brown, P. Maunz, L.-M. Duan, and J. Kim, Physical Review A **89**, 022317 (2014).

[3] N. Y. Yao, L. Jiang, A. V. Gorshkov, P. C. Maurer, G. Giedke, J. I. Cirac, and M. D. Lukin, Nat Commun **3**, 800 (2012), arXiv:1012.2864.

[4] N. H. Nickerson, J. F. Fitzsimons, and S. C. Benjamin, Physical Review X **4** (2014), 10.1103/PhysRevX.4.041041, arXiv:1406.0880.

[5] R. Raussendorf and H. J. Briegel, Physical Review Letters **86**, 5188 (2001).

[6] K. Kieling, T. Rudolph, and J. Eisert, Physical Review Letters **99**, 130501 (2007).

[7] M. Gimeno-Segovia, P. Shadbolt, D. E. Browne, and T. Rudolph, Physical Review Letters **115**, 020502 (2015).

[8] H. A. Zaidi, C. Dawson, P. Van Loock, and T. Rudolph, Physical Review A - Atomic, Molecular, and Optical Physics **91**, 042301 (2015), arXiv:1410.3753.

[9] D. E. Browne, M. B. Elliott, S. T. Flammia, S. T. Merkel, A. Miyake, and A. J. Short, New Journal of Physics **10**, 023010 (2008), arXiv:0709.1729.

[10] C. W. Chou, H. de Riedmatten, D. Felinto, S. V. Polyakov, S. J. van Enk, and H. J. Kimble, Nature **438**, 828 (2005).

[11] D. L. Moehring, P. Maunz, S. Olmschenk, K. C. Younge, D. N. Matsukevich, L.-M. Duan, and C. Monroe, Nature **449**, 68 (2007).

[12] R. Kolesov, K. Xia, R. Reuter, R. Stöhr, A. Zappe, J. Meijer, P. Hemmer, and J. Wrachtrup, Nature Communications **3**, 1029 (2012).

[13] H. Bernien, B. Hensen, W. Pfaff, G. Koolstra, M. S. Blok, L. Robledo, T. H. Taminiau, M. Markham, D. J. Twitchen, L. Childress, and R. Hanson, Nature **497**, 86 (2013), arXiv:1212.6136.

[14] B. Hensen, H. Bernien, A. E. Dréau, A. Reiserer, N. Kalb, M. S. Blok, J. Ruitenberg, R. F. L. Vermeulen, R. N. Schouten, C. Abellán, W. Amaya, V. Pruneri, M. W. Mitchell, M. Markham, D. J. Twitchen, D. Elkouss, S. Wehner, T. H. Taminiau, and R. Hanson, Nature **526**, 682 (2015), arXiv:1508.05949.

[15] N. Bar-Gill, L. Pham, A. Jarmola, D. Budker, and R. Walsworth, Nature Communications **4**, 1743 (2013).

[16] F. Dolde, V. Bergholm, Y. Wang, I. Jakobi, B. Naydenov, S. Pezzagna, J. Meijer, F. Jelezko, P. Neumann, T. Schulte-Herbrüggen, J. Biamonte, and J. Wrachtrup, Nature Communications **5**, 345 (2014).

[17] L. Childress, M. V. Gurudev Dutt, J. M. Taylor, A. S. Zibrov, F. Jelezko, J. Wrachtrup, P. R. Hemmer, and M. D. Lukin, Science **314** (2006).

[18] P. C. Maurer, G. Kucsko, C. Latta, L. Jiang, N. Y. Yao, S. D. Bennett, F. Pastawski, D. Hunger, N. Chisholm, M. Markham, D. J. Twitchen, J. I. Cirac, and M. D. Lukin, Science **336**, 1283 (2012), arXiv:arXiv:1202.4379v1.

[19] L. Robledo, L. Childress, H. Bernien, B. Hensen, P. F. Alkemade, and R. Hanson, Nature **477**, 574 (2011), arXiv:1301.0392v1.
[20] S. L. Mouradian, T. Schröder, C. B. Poitras, L. Li, J. Goldstein, E. H. Chen, M. Walsh, J. Cardenas, M. L. Markham, D. J. Twitchen, M. Lipson, and D. Englund, Physical Review X **5**, 031009 (2015).
[21] M. Z. Bazant, Physical Review E **62**, 1660 (2000).
[22] K. Kieling and J. Eisert, Lecture Notes in Physics **762**, 287 (2009), arXiv:0712.1836.
[23] M. Van Den Nest, A. Miyake, W. Dür, and H. J. Briegel, Physical Review Letters **97** (2006), 10.1103/PhysRevLett.97.150504, arXiv:0604010 [quant-ph].
[24] S. D. Barrett and P. Kok, Physical Review A **71**, 060310 (2005).
[25] Supplementary material.
[26] L. Li, E. H. Chen, J. Zheng, S. L. Mouradian, F. Dolde, T. Schröder, S. Karaveli, M. L. Markham, D. J. Twitchen, and D. Englund, Nano Letters **15**, 1493 (2015).
[27] J. P. Hadden, J. P. Harrison, A. C. Stanley-Clarke, L. Marseglia, Y.-L. D. Ho, B. R. Patton, J. L. O'Brien, and J. G. Rarity, Applied Physics Letters **97**, 241901 (2010).
[28] L. Li, T. Schr\"oder, E. H. Chen, M. Walsh, I. Bayn, J. Goldstein, O. Gaathon, M. E. Trusheim, M. Lu, J. Mower, M. Cotlet, M. L. Markham, D. J. Twitchen, and D. Englund, Nature Comm. **6**, 6173 (2015), arXiv:1409.1602.
[29] M. E. J. Newman and R. M. Ziff, Physical Review E - Statistical, Nonlinear, and Soft Matter Physics **64**, 1 (2001), arXiv:0101295 [cond-mat].
[30] S. R. Broadbent and J. M. Hammersley, Mathematical Proceedings of the Cambridge Philosophical Society **53**, 629 (1957).
[31] M. Sahimi, B. D. Hughes, L. E. Scriven, and H. T. Davis, J. Phys. A: Math. Gen. **16**, 67 (1983).
[32] M. Reck and A. Zeilinger, Physical Review Letters **73**, 58 (1994).
[33] Y. Shen, N. C. Harris, S. Skirlo, M. Prabhu, T. Baehr-Jones, M. Hochberg, X. Sun, S. Zhao, H. Larochelle, D. Englund, and M. Soljacic, arXiv.physics.optics **10**, 02365 (2016), arXiv:1610.02365.